Asian Journal of Pharmaceutical Sciences 20 (2025) 101016

Available online at www.sciencedirect.com

ScienceDirect

journal homepage: www.elsevier.com/locate/AJPS

Research Article

Codelivery of apigenin, FdUMP and CD276 antibody synergistic inhibit colorectal cancer by ferroptosis-apoptosis-pyroptosis and CD276 blockade

Weiran Cao[a,b,1], *Xue Zhang*[a,1], *Jiaxuan Chen*[a], *Lu Sun*[a], *Huining He*[a,*], *Fei Yu*[a,*]

[a] *Tianjin Key Laboratory on Technologies Enabling Development of Clinical Therapeutics and Diagnostics, International Joint Laboratory of Ocular Diseases, School of Pharmacy, School of Biomedical Engineering and Technology, Tianjin Medical University, Tianjin 300070, China*
[b] *Laboratory of Integrated Medicine Tumor Immunology, Shanxi University of Chinese Medicine, Taiyuan 030000, China*

ARTICLE INFO

Article history:
Received 14 September 2024
Revised 27 November 2024
Accepted 1 December 2024
Available online 4 January 2025

Keywords:
Mitochondria damage
DNA replication arrest
Immune-checkpoint blockade
Chemo-immunotherapy
Colorectal cancer treatment

ABSTRACT

Mitochondria provides adenosine triphosphate for multiple vital movements to ensure tumor cell proliferation. Compared to the broadly used method of inducing DNA replication arrest to kill cancer, inducing mitochondria damage to cause energy shortage is quite promising as it can inhibit tumor cell bioactivities, increase intracellular accumulation of toxic drugs, eventually sensitize chemotherapy and even reverse drug resistance. Breaking the balance of glutathione (GSH) and reactive oxygen species (ROS) contents have been proven efficient in destroying mitochondria respectively. Herein, apigenin, a GSH efflux reagent, and 2′-deoxy-5-fluorouridine 5′-monophosphate sodium salt (FdUMP) that could induce toxic ROS were co-delivered by constructed lipid nanoparticles, noted as Lip@AF. An immune-checkpoint inhibition reagent CD276 antibody was modified onto the surface of Lip@AF with high reaction specificity (noted as αCD276-Lip@AF) to enhance the recognition of immune cells to tumor. Results showed that the redox balance was destroyed, leading to severe injury to mitochondria and cell membrane. Furthermore, synergistic DNA/RNA replication inhibition caused by inhibiting the function of thymidylate synthase were observed. Eventually, significantly enhanced cytotoxicity was achieved by combining multiple mechanisms including ferroptosis, apoptosis and pyroptosis. *In vivo*, strengthen tumor growth inhibition was achieved by αCD276-Lip@AF with high biosafety, providing new sights in enhancing chemotherapy sensitiveness and achieving high-performance chemo-immunotherapy.

* Corresponding authors.
E-mail addresses: hehuining@tmu.edu.cn (H. He), feiyu@tmu.edu.cn (F. Yu).
[1] These authors contributed equally to this work.
Peer review under responsibility of Shenyang Pharmaceutical University.

https://doi.org/10.1016/j.ajps.2025.101016

1. Introduction

Mitochondria acts as the energy supply factory of cells, providing adenosine triphosphate (ATP) for multiple vital movements including DNA replication, protein synthesis, and exogeneous drug efflux [1]. Mitochondrial dysfunction with energy shortage was regarded as a promising antineoplastic strategy than the broadly used method of inhibiting DNA replication, which could simultaneously promotes cell proliferation arrest and sensitizing chemotherapy-induced cell apoptosis [2–3]. Recently, ferroptosis, a cell death type characterized by severely mitochondrial shrinkage and membrane density increase, was reported to damage mitochondria by disrupting intracellular redox balance [4–5]. Peroxidative environment promotes the oxidation of bio-membranes and release of high-immunogenic molecules, ultimately enhancing the immunogenicity of tumors [6]. Therefore, more effector T cells and natural killer cells were recruited and infiltrated into tumor microenvironment, which sensitives the therapeutic efficacy of immune-checkpoint inhibitors (ICIs). Eventually, by combining ferroptosis inducers with ICIs, *in situ* tumor depletion and distant metastasis inhibition were efficiently achieved.

5-fluorouracil (5-FU) is broadly applied in colorectal cancer (CRC) treatment [7]. After uptake by tumor cells, 5-FU transformed to 5-fluoro-2′-deoxyuridine 5′-monophosphate sodium salt (FdUMP), its intracellular active form [8]. FdUMP exerts cytotoxicity by upregulating the content of toxic reactive oxygen species (ROS) or inducing cell proliferation arrest *via* specific binding with thymidylate synthase (TS) [8]. To further magnified the oxidation damage to mitochondria by FdUMP-induced ROS, highly expressed intracellular antioxidant system, *e.g.*, glutathione (GSH) or glutathione peroxidase 4 (GPX4) [9], were need to be depleted. Apigenin has been reported efficient in GSH efflux [10], and the enhanced therapeutic efficiency after apigenin added to 5-FU was verified in multiple disease models including cancers [11–13]. Furthermore, apigenin could downregulate the expression of TS, achieving synergistic anti-proliferation effect by inducing apoptosis [14] combined with the irreversible binding capacity of FdUMP [15–18]. By this way, cell ferroptosis and apoptosis were occurred. CD276, an immune-checkpoint molecule highly expressed on tumor cell surface [19–21], was proved associated with various aspects of disease progression and poor prognosis [22]. We blocked CD276 by its corresponding antibody to enhance the recognition of infiltrated $CD8^+$ T cells [23] and adaptive immunity mediated tumor elimination [24], simultaneously decrease the CRC cell resistance to ferroptosis [25].

Herein, lipid nanoparticles with calcium phosphate (CaP) inner core were constructed for codelivery of apigenin, FdUMP and CD276 antibody (αCD276), noted as αCD276-Lip@AF. Drugs were encapsulated by rationally utilizing their structural properties. *In vitro*, efficient damage to cell mitochondria and cell membrane were shown by disrupting intracellular redox homeostasis, the downregulation of GSH and the DNA replication injury resulted in severe cell proliferation arrest. *In vivo*, after effectively accumulated at tumor site, strengthen tumor inhibition was achieved in αCD276-Lip@AF treated group, indicating the synergistic antineoplastic efficiency of chemical drugs induced cell injury combined with immune-checkpoint inhibitor mediated immunotherapy, providing new insights into the therapy of malignant tumors including CRC.

2. Materials and methods

2.1. Materials

Apigenin was purchased from HEOWNS (purity 98 %, Shanghai, China). FdUMP was obtained from Sigma Adrich (purity 85 %, USA). CD276 antibody was purchased from BioxCell (USA). 1,2-dioleoyl-sn–glycero-3-phosphate (DOPA) was purchased from Aladdin (Shanghai, China). DOTAP was purchased from Xi'an ruixi Biological Technology Co., Ltd (Xi'an, China). Cholesterol was purchased from Rhawn (Shanghai, China). N-(Carbonyl-methoxypolyethyleneglycol 2000)−1,2-distearoyl-sn–glycero-3-phosphoethanolamine ($DSPE\text{-}PEG_{2000}$) was purchased from AVITO Pharmaceutical Technology Co., Ltd (Shanghai, China). DSPE-PEG-Maleimide (DSPE-PEG-Mal) was purchased from Avanti lipids (USA). Ethanol and dichloromethane were purchased from Tianjin Jiangtian Chemical Technology Co., Ltd. (Tianjin, China).

2.2. Sulfhydryl modification on CD276 antibody

CD276 antibodies were diluted into pH 8.0 PBE solution (containing 2 mM EDTA), 2 mg/mL Trauts' reagent was added. The sulfhydryl reaction was processed at room temperature (r.t.), 130 rpm stirring for 2 h, with a 1: 10 molar ratio of CD276 antibody to Trauts' reagent. At the end of reaction, excess Trauts' reagent was removed by dialysis within pH 7.4 PBS solution. The resultant sulfhydryl modified CD276 antibodies were stored at 4 °C for further use.

2.3. Preparation and characterization of αCD276-Lip@AF

Lipid nanoparticles with calcium phosphate core were utilized for codelivery of apigenin, FdUMP and αCD276. Reverse phase microemulsion method described in previous studies [26] was employed as follows. Briefly, 100 μl FdUMP stock solution (1 mg/ml) and 5 μl $(NH_4)_2HPO_4$ solution (concentration = 0.5 M) were mixed thoroughly and the pH was adjusted to 10.0 to obtain 'P phase solution', then 'P phase solution' was added into 5 ml microemulsion solution composed of cyclohexane and Igepal CO-520 with a volume ratio of 7: 3 to form emulsion A. 100 μl $CaCl_2$ solution (concentration = 2.5 M), referred as 'Ca phase solution', was added into another 5 ml microemulsion solution and mixed thoroughly to form emulsion B. Next, two emulsions were mixed and 25 μl DOPA stock solution (100 mg/ml) was added. The mixture was stirred for 15 min, equal volume of pure ethanol was added and washed for another 15 min. After ethanol wash, the mixture was centrifugated at 10,000 rpm for 20 min, the precipitation was collected, 1.5 μl apigenin stock solution (10 mg/ml in DMSO), 56 μl lipids stock solution (DOTAP: Cholesterol: DSPE-PEG: DSPE-PEG-Mal = 40: 40: 16: 4) and 5 ml dichloromethane were added. Organic solvents were removed through rotary

evaporation, 2 ml PBS solution was added and sonicated to form lipid nanoparticles encapsulated apigenin and FdUMP (Lip@AF). Subsequently, sulfhydryl modified CD276 antibodies were added and cultured at r.t. for 2 h to form αCD276-Lip@AF. The resulted formulation was filtered through 0.45 μm and stored at 4 °C without further purification.

The morphology of Lip@F, Lip@AF, αCD276-Lip@F and αCD276-Lip@AF were observed by transmission electron microscopy (TEM, Hitachi HT7700). The dynamic size distribution and ζ potential of formulations was determined by dynamic light scattering (DLS, NanoZS 90) and calculated by software. The serum stability was evaluated by incubating the αCD276-Lip@AF samples into 10 % (v/v) fetal bovine serum (FBS, BI, Isreal) for 0, 1, 4 and 10 h, the size and ζ potential change were determined and compared.

2.4. Cell culture and cell viability assay

Murine colorectal cancer cell line (CT26 cells) was obtained from School of Pharmacy of Tianjin Medical University. DMEM medium (Gibco, USA) supplemented with 10 % (v/v) FBS and 1 % (v/v) antibiotic-antimycotic (Gibco, USA) was utilized for CT26 culture, with 37 °C incubation temperature, 5 % CO_2 and 95 % humidity atmosphere.

Relative cell viability after various treatments were assessed using standard 3-(4,5-dimethylthiazol-2-yl)−2,5-diphenyltetrazolium bromide (MTT, Meilunbio, Dalian, China) assay. Cells were seeded into 96-well plates at density of 1×10^4 per well, and incubated at 37 °C overnight. Drugs were added next day and cocultured for additional 24 h. Subsequently, 20 μl MTT solution (5 mg/ml) was added for 4 h. Then, the medium was removed and 150 μl DMSO was added, shaking at 100 rpm for 15 min and avoiding light. Absorbance at 570 nm was measured for calculating half inhibition concentration (IC_{50}) by GraphPad Prism software.

2.5. Intracellular ROS detection

The capacities of PBS, free FdUMP, free apigenin, free apigenin + FdUMP, Lip@F, Lip@AF in inducing intracellular ROS were validated using DCFH-DA probes (Solarbio, Beijing, China). Cells were seeded into 6-well plates with density of 1×10^5 per well and cultured overnight for adherence. Then free drugs or formulations ($[C]_{FdUMP} = 0.5$ μM, $[C]_{Apigenin} = 0.1$ μM) were added for 24 h, subsequently DCFH-DA probes were loaded for 20 min. The green fluorescence from oxidized DCF was observed using Inverted Fluorescence Microscopy (IFM) and quantified by ImageJ software.

2.6. Cell membrane lipids peroxidation

CT26 cells were seeded into 6-well plates with density of 3×10^5 per well. Cells were incubated overnight and added with PBS, free apigenin, free FdUMP, free apigenin + FdUMP, Lip@F, Lip@AF at equivalent concentration of 0.5 μM FdUMP and 0.1 μM apigenin for 24 h. Subsequently, cells were cocultured with 1 μM Liperfluo probe (GlpBio, USA) for 30 min. After that, cells were fixed with 4 % PFA and washed with PBS twice. The green fluorescence of LiperfluoOX was observed by IFM and quantified by ImageJ software.

2.7. Cell proliferation arrest test

Cell proliferation disruption was determined using the EdU Cell Proliferation Image Kit (Abbkine, USA). CT26 cells were seeded into 6-well plates with density of 1×10^5 per well. After overnight incubation, cells were treated with PBS, free FdUMP, free apigenin, free FdUMP + apigenin, Lip@F and Lip@AF and cocultured for 24 h ([c] of FdUMP was 75 ng/ml; [c] of Apigenin was 11.25 ng/ml). Then cells were washed with PBS twice and EdU was added at 37 °C for 2 h to incorporated into genomic DNA. After fixed by 4 % PFA and permeated by Triton-X 100, anti-EdU antibody and DAPI was added for labeling DNA and nucleus. The EdU positive cells were observed by IFM and positive cell ratios were quantified using ImageJ software. The experiments were repeated independently 3 times.

2.8. Annexin-V and propidium iodide (PI) staining

CT26 cells were incubated into 6-well plates with density of 3×10^5 per well. After overnight culture, cells were added with PBS, free apigenin, free FdUMP, free apigenin + FdUMP, Lip@F, Lip@AF at equivalent concentration of 0.5 μM FdUMP and 0.1 μM apigenin for 24 h. Then cells were fixed with 4 % PFA for 20 min, stained with Annexin-V for 15 min and PI for 5 min (Meilunbio, China). Apoptosis cells were observed and captured using IFM.

2.9. Cell swelling phenotype and JC-1 assay

The swelling phenotype of treated cells was observed and recorded by IFM. Briefly, cells were seeded into 6-well plates with density of 2.5×10^5 per well and incubated overnight. Next day, PBS, Lip@F, Lip@AF at the equivalent FdUMP concentration of 0.5 μM were added and co-cultured for 12 h. Represented images from different groups were recorded.

CT26 cells were seeded into 6-well plates with density of 2×10^5 per well. Cells were incubated overnight, subsequently PBS, Lip@F, αCD276-Lip@F, Lip@AF, αCD276-Lip@AF were added at equivalent concentration of 0.5 μM FdUMP and 0.1 μM apigenin for 12 h. The culture media was replaced with fresh media, JC-1 staining buffer containing JC-1 probe (Abbexa, UK) was added and cocultured at 37 °C for 20 min. After washed with fresh staining buffer twice, the fluorescence was observed by IFM.

2.10. GSH and MDA content detection

CT26 cells were seeded into 6-well plates with density of 5×10^4 per well. Cells were incubated overnight and PBS, Lip@F, αCD276-Lip@F, Lip@AF, αCD276-Lip@AF were added at equivalent concentration of 0.5 μM FdUMP and 0.1 μM apigenin for 12 h. Then the media were separated and centrifugated at 1,000 rpm for 3 min. The supernatants were collected as extracellular samples. The cell precipitations were resuspended into MES buffer and added into their prior well, respectively. The 6-well plate was sonicated 2 min for extracting intracellular GSH, and solutions were obtained after sonication as intracellular samples. Then, 50 μl samples were added into 96-well plate and mixed with 150 μl cocktail

mixture (Cayman Chemical, USA). The plate was stirred at 37 °C, 130 rpm for 25 min. Absorbance at 412 nm were detected for calculating relative GSH contents.

CT26 cells were seeded into 6-well plate with density of 2×10^5 per well and incubated overnight. Next day, PBS, Lip@F, αCD276-Lip@F, Lip@AF, αCD276-Lip@AF were added at equivalent concentration of 0.5 μM FdUMP and 0.1 μM apigenin for 24 h. Cells were washed with fresh media, collected by centrifugation, resuspended into fresh PBS, and counted using CountStar software (Alit Lifetech Co., Limited). Cells were centrifugated again, then added with 150 μl extraction buffer, sonicated by 20 % power for 5 min (sonicated 3 s and stopped for 7 s with total 30 cycles). Then, after centrifugation at 13,000 × g (4 °C) for 10 min, the supernatants were collected and put into metal bath for 30 min. MDA contents were determined according to the reagent instructions (DOJINDO, Japan).

2.11. *Animals*

Four to six weeks old male Balb/C mice were purchased from Charles River Co., Ltd (Beijing, China). Mice were fed in SPF environment with 12 h/12 h bright/dark cycle. Food and water were allowed *ad libitum*. Before starting the experiments, animals were fed at least one week.

2.12. *In vivo biodistribution evaluation*

CT26 cells were injected at right flank of Balb/C mice to establish subcutaneous murine colorectal cancer models. Then mice were injected via tail vein with PBS, DiR labelled Lip@AF and DiR labelled αCD276-Lip@AF, 3 mice per group. After injection at 2, 4, 6, 8 and 24 h, mice were imaged at IVIS® SPECTRUM (PerkinElmer, USA) with Em/Ex = 680 nm/720 nm to observe the time-dependent *in vivo* biodistribution of drugs. 24 h after injection, mice were sacrificed and hearts, livers, spleens, lungs, kidneys and tumors were collected for observing the *ex vivo* biodistribution of fluorescence intensities. Statistical analysis was performed by Living Image Software.

2.13. *In vivo administration dose optimization*

Mice were injected with different doses of αCD276-Lip@AF via tail vein. After administered with equivalent dose of 250, 500, 750 μg/kg FdUMP, the bio-status of mice were observed the next day. In terms of mice status, the proper injection dose was selected.

2.14. *In vivo anti-tumor efficiency assessment*

CT26 cells were injected at the right flank of mice at Day 7, and the mice were weighed for grouping. The tumor bearing mice were continuously observed. At Day 0, the tumor volumes and mice body weights were determined for comparison of the difference among groups. At Day 0, 3 and 6, mice were injected via tail vein with PBS, free FdUMP + apigenin, Lip@AF, αCD276-Lip@A, αCD276-lip@F and αCD276-Lip@AFrespectively, and the tumor volumes and body weights were measured every 3 d to draw the curves. At Day 15, mice blood was collected by retro-orbital puncture of anesthetized mice, the contents of blood urine (BUN), serum creatinine (Scr), alanine aminotransferase (ALT) and aspartate aminotransferase (AST) in serum were determined to evaluate the *in vivo* biosafety after preparing the standard fitting curves. Then, mice were sacrificed using excessive isoflurane and the images were captured. Tumors were collected, imaged and weighed to calculate the tumor inhibition rate (TGI%). After dehydration and fixation for 24 h, tumors were embedded with OCT (Sakura, Japan) and sectioned to 8 μm, the tumor necrosis, apoptosis and proliferation arrest were evaluated by Hematoxylin-Eosin (H&E), Terminal-Deoxynucleotidyl Transferase-Mediated Nick End Labeling (TUNEL) and Ki67 staining, respectively. Normal organs were embedded and H&E staining was performed for further *in vivo* biosafety evaluation.

2.15. *Statistical analysis*

All experiments were repeated independently at least 3 times. Results were shown as the mean ± standard deviation (SD). Statistical analysis was performed using GraphPad Prism software. The difference between groups were analyzed using students' t tests (for two groups) and one-way analysis of variance (One-way ANOVA, for at least three groups). Two-way analysis of variance (Two-way ANOVA) followed with sidak's multiple comparisons test was applied for multiple sub-column comparisons across groups.

3. Results and discussion

3.1. *Preparation and characterization of αCD276-Lip@AF*

The chemical conjugation of antibody on surface was reported more sensitive to antigens compared with physical adsorption method [27]. Therefore, the click chemistry-based chemical link was chosen for antibody conjugation in this study, by reacting sulfhydryl and maleimide with high specify [28–30]. As shown in Fig. 1A, sulfhydryl was incorporated into αCD276 through Trauts' reagent, with averaged 3.3 sulfhydryl modified on one antibody's surface (Step 1), the maleimide group in DSPE-PEG-Mal was selected as the antibody surface modification site. Electrostatic attraction between phosphate group with calcium ion (2+) was utilized for encapsulation of FdUMP into core, while apigenin was wrapped into the lipophilic lipid membrane (Step 2). These two chemical drugs could be totally encapsulated by utilizing optimized preparation method described in previous work, and the loading capacity was calculated as 0.70 % for FdUMP and 0.10 % for apigenin. Lipid nanoparticles encapsulated single FdUMP, FdUMP plus apigenin, αCD276 plus FdUMP, αCD276 plus apigenin and all the three drugs were defined as Lip@F, Lip@AF, αCD276-Lip@F, αCD276-Lip@A and αCD276-Lip@AF, respectively. The TEM image exhibited the spheric shape of αCD276-Lip@AF (Fig. 1B) which was accordance with Lip@A, Lip@F and Lip@AF (Fig. S1). The averaged diameters were measured by DLS, showing the similar size of Lip@F (125.80 ± 2.65 nm) and Lip@AF (134.60 ± 0.97 nm) which were approximately 25 - 34 nm smaller than αCD276-

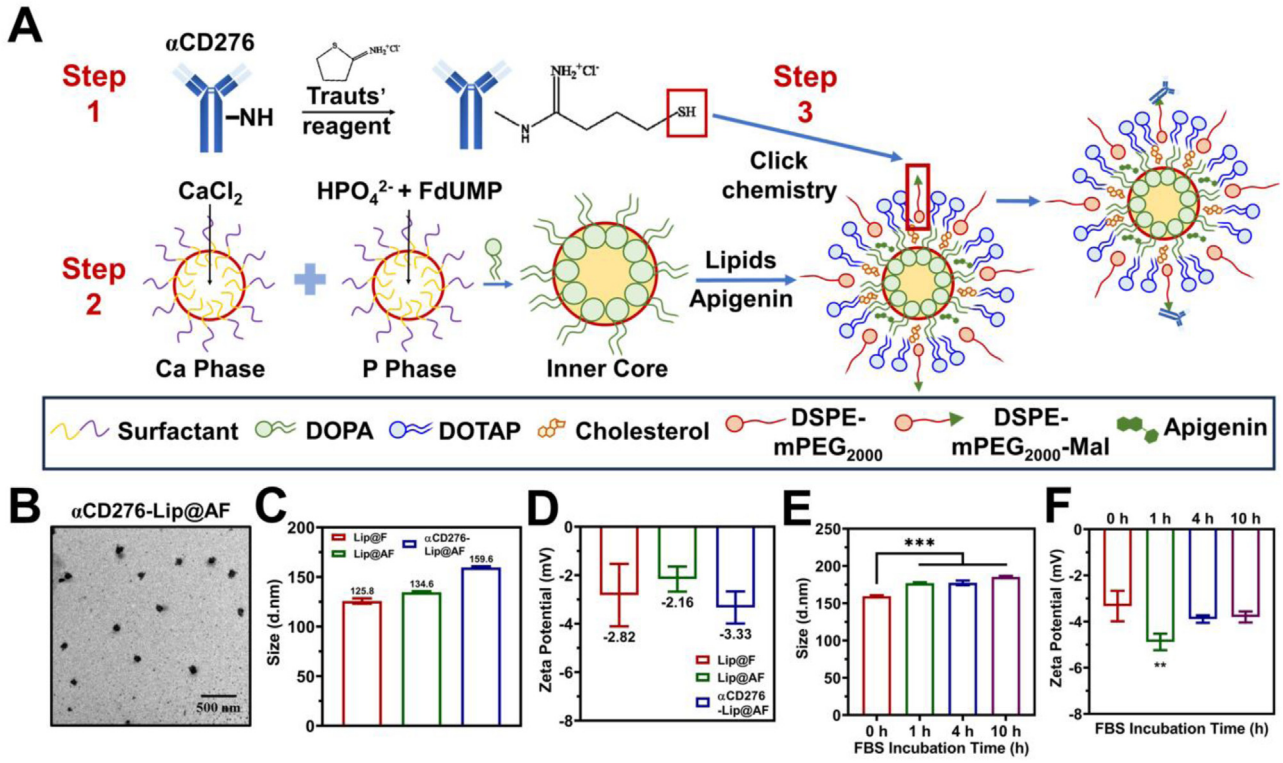

Fig. 1 – Preparation and characterization of αCD276-Lip@AF. (A) Schematic illustration of the preparation procedure of αCD276-Lip@AF; (B) TEM image of αCD276-Lip@AF (bar = 500 nm); (C) Averaged diameter and (D) averaged ζ potentials of Lip@F, Lip@AF and αCD276-Lip@AF ($n = 3$); (E) Size and F) ζ potential change after incubated with 10 % (v/v) FBS up to 10 h ($n = 3$, $^{**}P < 0.01$, $^{***}P < 0.001$).

Lip@AF (159.60 ± 1.16 nm) (Fig. 1C and S2), demonstrating the successful surface conjugation of αCD276. Whereas, the number% diameters of the three samples were all nearly 70 nm with no significant difference (Fig. S2). The ζ potentials of LNPs were determined to be nearly −3 mV (−2.82 ± 1.29 mV for Lip@F, −2.16 ± 0.52 mV for Lip@AF and −3.33 ± 0.66 mV for αCD276-Lip@AF), independent with the antibody modification (Fig. 1D and S2). The size and PDI variance of αCD276-Lip@AF after incubated in 10 % (v/v) FBS was determined for simulating its stability in blood circulation. In a 10 h incubating period, the size slightly increased (~159.57 nm at 0 h point; ~185.30 nm at 10 h point), which was mostly progressed within 1 h (177.07 nm at 1 h point) (Fig. 1E, $^{***}P < 0.001$). Similarly, the PDI showed a sudden increase within 1 h ($^{**}P < 0.01$) and a slow increase trend up to 10 h ($^{***}P < 0.001$) (Fig. S3). The nearly steady ζ potentials (final steady to −3.80 mV at 10 h point) demonstrated the minor formation of protein corona due to the slightly protein adsorption (Fig. 1F). These above results indicated the promising stability of αCD276-Lip@AF in serum.

3.2. *Synergistic antineoplastic efficiency of apigenin combined with FdUMP*

The *in vitro* combination cytotoxicity and anti-tumor mechanisms of apigenin plus FdUMP were evaluated first on mouse CRC cell line (CT26 cell). MTT results showed the IC_{50} value of Lip@AF was calculated to be ~ 0.60 ± 0.09 μM, 1.5 folds lower than that of Lip@F (~ 0.92 ± 0.01 μM), exhibiting the significantly enhanced cytotoxicity of this combination drugs ($^{*}P = 0.0187$) (Fig. 2A and S4). Depleted intracellular GSH by apigenin combined with induced ROS by FdUMP resulted in severe redox imbalance. We first detected the overall intracellular ROS after treatments by DCFH-DA probe. Obviously stronger green fluorescence was seen in Lip@AF treated group (Fig. 2B and S5), approximately 2.85-fold higher than free FdUMP, free apigenin and their physical mixture (free apigenin + FdUMP) treated group according to fluorescence intensity statistical results (Fig. S6). Overproduced toxic ROS could lead to the peroxidation of membrane lipids. Herein, Liperfluo probe was utilized for intracellular ROS detection, which could emit strong green fluorescence after oxidation presented as LiperfluoOX form. Higher level of green fluorescence was seen in Lip@AF treated group (Fig. 2C and S7), approximately 15-fold compared with control group ($^{***}P < 0.001$) (Fig. S8), indicating the higher degree of lipid oxidation by ROS. Additionally, the cell proliferation arrest assay was conducted using EdU probe to investigate the anti-proliferation ability of apigenin and FdUMP. Results showed in Lip@AF treated group, significant less DAPI stained cells (Fig. 2D) as well as lower ratio of EdU positive cells (Fig. S9, Lip@AF group 44.53 % vs PBS group 53.74 %) were observed, demonstrating their combinational capacity of inducing proliferation arrest and cell death. In a

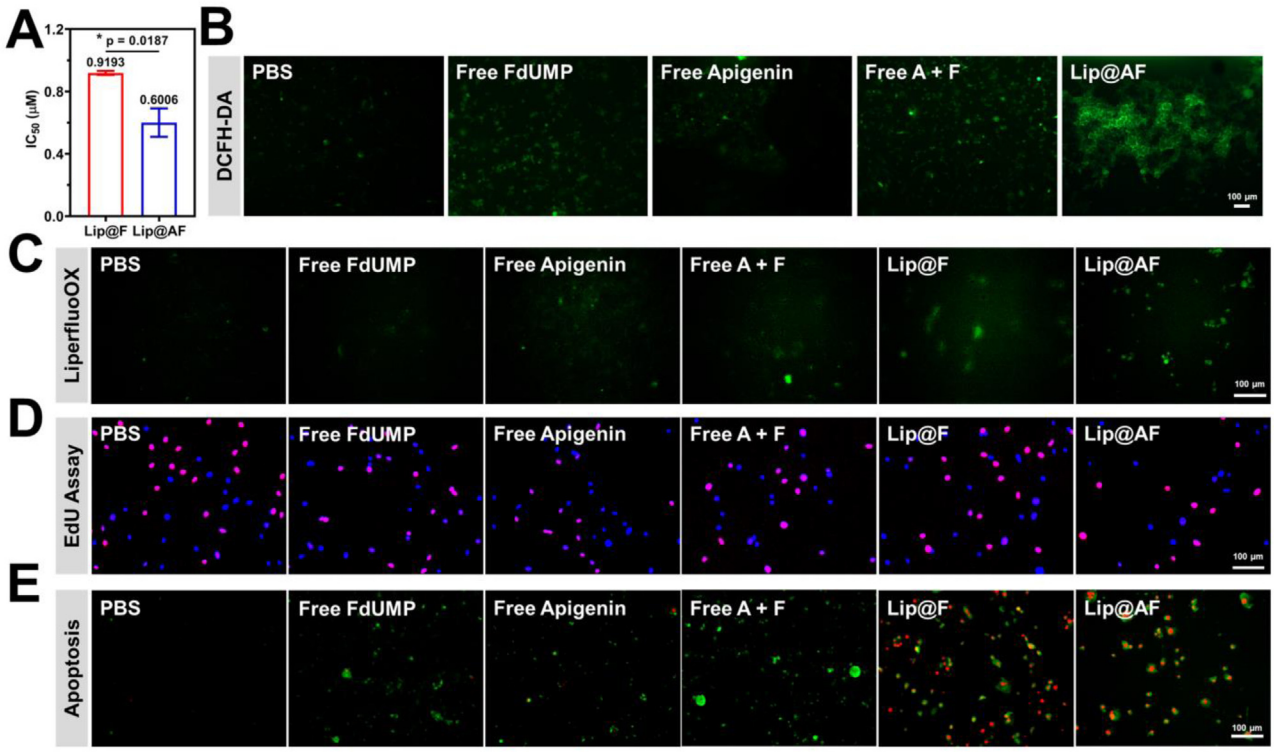

Fig. 2 – *In vitro* evaluation of Lip@AF on CT26 cells. (A) IC_{50} values of Lip@F and Lip@AF by MTT assay; (B) Intracellular ROS detected by DCFH-DA probe (Scale bar: 100 μm); (C) The peroxidation degree of lipids detected by LiperfluoOX probe (Scale bar: 100 μm); (D) Evaluation of cell proliferation arrest by EdU probe (Scale bar: 100 μm); E) Evaluation of cell apoptosis by Annexin-V/PI staining (Scale bar: 100 μm). All experiments were parallel processed 3 times.

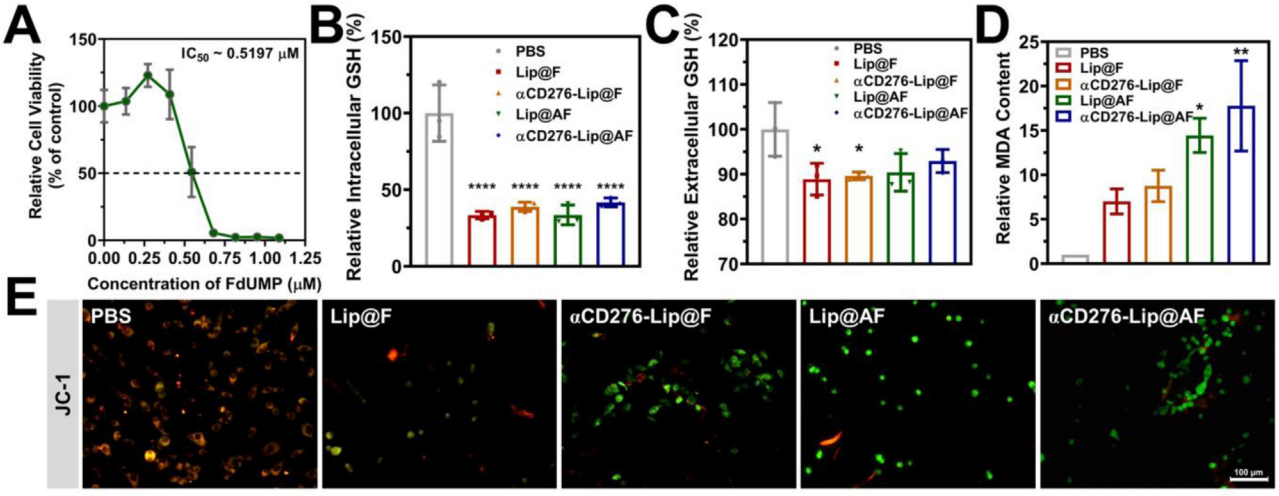

Fig. 3 – *In vitro* evaluation of αCD276-Lip@AF on CT26 cells. (A) IC_{50} values of αCD276-Lip@AF by MTT assay; (B) Intracellular GSH contents after treatments detected by Ellmans' reagent; (C) Extracellular GSH contents after treatments detected by Ellmans' reagent; (D) Relative intracellular MDA contents after treatments; (E) The mitochondria membrane potential change after treatments detected by JC-1 reagent (bar: 100 μm) (*P < 0.05, ** P < 0.01, ****P < 0.0001). All experiments were parallel processed 3 times.

separate experiment, cell apoptosis after various treatments were assessed by annexin-V/PI staining. Simultaneous nuclear staining by PI and cell membrane staining by Annexin-V indicated the late-stage cell apoptosis, which could be observed in Lip@F and Lip@AF group (Fig. 2 and S10). Apart from this, more severe cytoplasm contraction was induced by Lip@AF, which may be caused by destruction of cell membrane. Therefore, the cellular morphology after treatments were observed under bright field (Fig. S11). The cell swelling phenotype, regarded as a morphology marker of cell pyroptosis, was seen only in Lip@AF group (Fig. S11), demonstrating cell membrane damage and as a result the outflow of cytoplasm, which was accordance with the results seen in apoptosis assay. These above preliminary *in vitro* results verified the powerful anti-tumor effects of FdUMP plus apigenin through multiple cell death mechanisms, including ferroptosis, apoptosis and pyroptosis.

3.3. *Antineoplastic efficiency assessment of αCD276-Lip@AF*

The CD276 antibody was conjugated on surface of Lip@AF through sulfhydryl-maleimide based click chemistry reaction. The cytotoxicity of αCD276-Lip@AF on CT26 cells was determined first for comparison with Lip@AF by MTT assay. The IC_{50} value was calculated to be ∼ 0.52 μM (Fig. 3A), slightly lower than that of Lip@F (∼ 0.60 ± 0.09 μM). Then, intracellular GSH efflux efficiencies by multiple treatments were evaluated (Fig. 3B). Efficient downregulation of GSH were observed among all treated groups (**** vs control, $P < 0.0001$). Due to the high cytotoxicity of FdUMP, the assay was processed with a low drug administration concentration, therefore the relatively low administered apigenin resulted in minor effects on intracellular GSH depletion, reflected as the minor difference between treated groups. We further assessed the extracellular GSH contents for additional analysis (Fig. 3C). Results showed in Lip@F and αCD276-Lip@F treated group, extracellular GSH contents were significantly lower (* vs control, $P < 0.05$), which may due to the transportation of GSH into cells for neutralizing the FdUMP-induced ROS. As for Lip@AF and αCD276-Lip@AF group, the extracellular GSH contents increased slightly after the codelivery of apigenin with FdUMP, verifying its GSH efflux capacity (Fig. 3C). The redox imbalance in cells finally lead to the peroxidation of lipids in multiple membranes, including cell membrane. MDA was a degradation product of lipid peroxidation, commonly used for assessment of the peroxidation degree. MDA contents after treatments were determined (Fig. 3D) and the contents in Lip@AF and αCD276-Lip@AF were significantly higher (* of Lip@AF vs control, $P < 0.05$, ** of αCD276-Lip@AF vs control, $P < 0.01$), demonstrating the higher degree of redox imbalance assisted with the better GSH efflux and ROS induction capacities. Additionally, overproduced ROS could lead to the decreased membrane potential as well as mitochondria damage, assessed by JC-1 probe (Fig. 3E and S12). Damaged mitochondria with low potential could be stained as green fluorescence (in JC-1 probe monomer form), which could be observed in αCD276-Lip@AF treated group compared with control. These above results verified the capacity of αCD276-Lip@AF in inducing redox imbalance and cell death.

3.4. *In vivo and ex vivo biodistribution evaluation*

Rational design and optimization of drug delivery systems benefit for achieving efficient tumor accumulation, which act as the prerequisite of the efficient tumor growth inhibition. By utilizing optimized preparation parameters in terms of previously published works [31,32], we constructed Lip@AF with relatively small diameters and narrow PDI distribution, and the *in vivo* and *ex vivo* biodistribution of Lip@AF and αCD276-Lip@AF were compared through real-time fluorescence imaging system (Fig. 4A). According to the images obtained at 2 h, 4 h, 6 h, 8 h and 24 h after *i.v.* injection of drugs, Lip@AF and αCD276-Lip@AF could rapidly accumulated at tumor sites, whereas the accumulation speed was independent on the antibody surface conjugation. We further assessed the *ex vivo* biodistribution 24 h after drug administration (Fig. 4B), and the fluorescence intensity per gram of tissues (ROI/g) were calculated for comparison (Fig. 4C). Surprisingly, Lip@AF accumulated mainly at spleens (**** vs control, $P < 0.0001$), far higher than that of livers (*** vs control, $P < 0.001$) and lungs (ns). The accumulation amount at tumors were basically equal to that of livers, showing a relatively high passive tumor targeting ability (** vs control, $P < 0.01$). As for αCD276-Lip@AF, αCD276 surface conjugation significantly decreased the distribution amount of Lip@AF at spleens (** vs Lip@AF, $P < 0.01$), while in livers and tumors, no significant difference was shown. We thought this phenomenon may be owing to the specific break of HS-Mal link in tumor microenvironment within high GSH contents, therefore the antibodies separated rapidly from the surface of Lip@AF, eventually resulting in less assistance for recognition between Lip@AF and tumor cells.

3.5. *In vivo anti-tumor efficiency evaluation*

Encouraged by the satisfied *in vitro* cytotoxicity and efficient *in vivo* tumor accumulation of αCD276-Lip@AF, next we evaluated the *in vivo* therapeutic efficiency against CRC, various treatments including PBS, free FdUMP + apigenin, Lip@AF, αCD276-Lip@A, αCD276-Lip@F and αCD276-Lip@AF were set as comparison groups. The schematical illustration of experiment process was shown in Fig. 5A. At Day 7, mice were inoculated with CT26 cells and grouped. Seven days after cell inoculation, the initial tumor volumes (Fig. S13) and body weights (Fig. S14) were measured. No significant difference was observed among groups, indicating the uniform dividing of CRC tumor bearing mice. Subsequently, drugs were *i.v.* administered every 3 d for 3 times. The final injection dose (equivalent to FdUMP) was optimized as 250 μg/kg; hindlimb weakness, blood urine/tail blackening would occur when mice injected with 750 μg/kg or 500 μg/kg FdUMP, respectively. Tumor volumes (Fig. 5B and S15) and mice body weights (Fig. S16) were recorded throughout the entire process until Day 15. After various treatments, the growth of tumors was inhibited in different extents; Lip@AF was verified better in tumor inhibition compared with free drug mixtures, indicating the enhanced tumor accumulation of drugs assisted with the lipid nanocarrier. The addition of αCD276 antibody exhibited stronger tumor inhibition by blocking immune-checkpoint CD276, and the codelivery of all

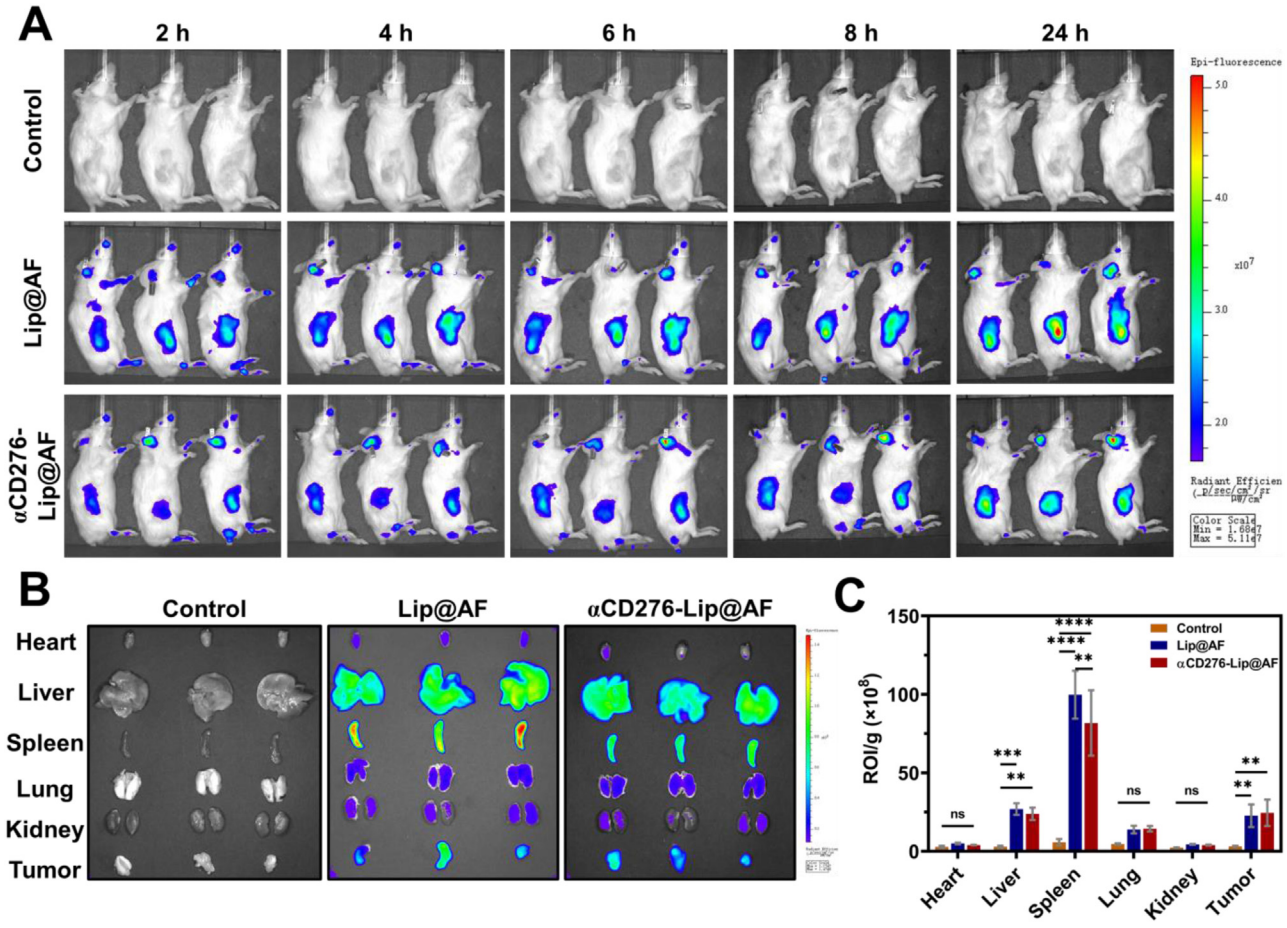

Fig. 4 – *In vivo* and *ex vivo* biodistribution of Lip@AF and αCD276-Lip@AF. (A) Real-time *in vivo* biodistribution of Lip@AF with or without antibody surface modification ($n = 3$); (B) Fluorescence images of *ex vivo* tissues obtained 24 h after drug *i.v.* injection ($n = 3$); (C) The statistical results of fluorescence intensity in *ex vivo* tissues (ns: no significance, ** $P < 0.01$, *** $P < 0.001$, **** $P < 0.0001$).

three drugs (αCD276-Lip@AF) significantly enhanced tumor growth control, resulting in a nearly horizontal growth curve compared to the Lip@AF treated group. The steadily increased mice body weights preliminary demonstrated the *in vivo* safety at this administered doses. At Day 15, the averaged tumor volumes of mice in various groups were compared (Fig. 5C). The tumor volumes in control, free drug mixtures, Lip@AF, αCD276-Lip@A, αCD276-Lip@F and αCD276-Lip@AF were reached nearly 1,500 mm^3, 970 mm^3, 649 mm^3, 562 mm^3, 388 mm^3 and 148 mm^3, respectively, significant treatment superiority of αCD276-Lip@AF over multiple groups was marked by asterisks. Then, mice were sacrificed, the image of tumor bearing mice was captured (Fig. S17), tissues and tumors were collected (Fig. S18), and tumor weights (Fig. 5D) were measured for calculation of tumor inhibition rate (TGI%, Fig. 5E). Significant tumor inhibition (41.93 % TGI) was observed in free drug mixture treated group (free FdUMP + apigenin), indicating the high antitumor efficiency of this combination even in free form. Passive targeted delivery of drugs with assistance of nanoparticles (Lip@AF) by enhanced permeability and retention effect (EPR) increased their tumor accumulation amount, eventually achieved better outcome (52.82 % TGI). CD276 blockade enhanced the tumor inhibition of chemical drug, as the mice treated with αCD276-Lip@AF exhibited the greatest tumor volume growth control (81.54 % TGI) compared with Lip@AF (52.82 % TGI, $P = 0.1491$), αCD276-Lip@A (46.60 % TGI, $P = 0.0542$) and αCD276-Lip@F (68.71 % TGI, $P = 0.8109$), indicating the enhanced immune recognition by blocking the immune-checkpoint. Next, H&E staining (Fig. 5F), TUNEL staining (Fig. 5G) and Ki67 staining (Fig. 5H) were performed for evaluating tumor necrosis, apoptosis and proliferation arrest. For αCD276-Lip@AF group, obvious unclear nuclear cytoplasmic boundary, cytoplasm contraction in H&E images and strong green fluorescence of TUNEL signal indicates the severe cell necrosis and apoptosis, almost unobservable Ki67 signal means the almost stagnant cell proliferation status. The *in vivo* biosafety of αCD276-Lip@AF was furtherly evaluated by determining blood biochemical indicators (Fig. 5I-L) utilizing standard fitting curves (Fig. S19) and investigating H&E staining (Fig. S20). Almost unchanged serum creatinine (Scr, ns vs control), blood urine nitrogen (BUN, ns vs control), slightly increased alanine aminotransferase (ALT, ns vs control) and decreased aspartate aminotransferase (AST, ~10.81 IU/l in αCD276-Lip@AF treated

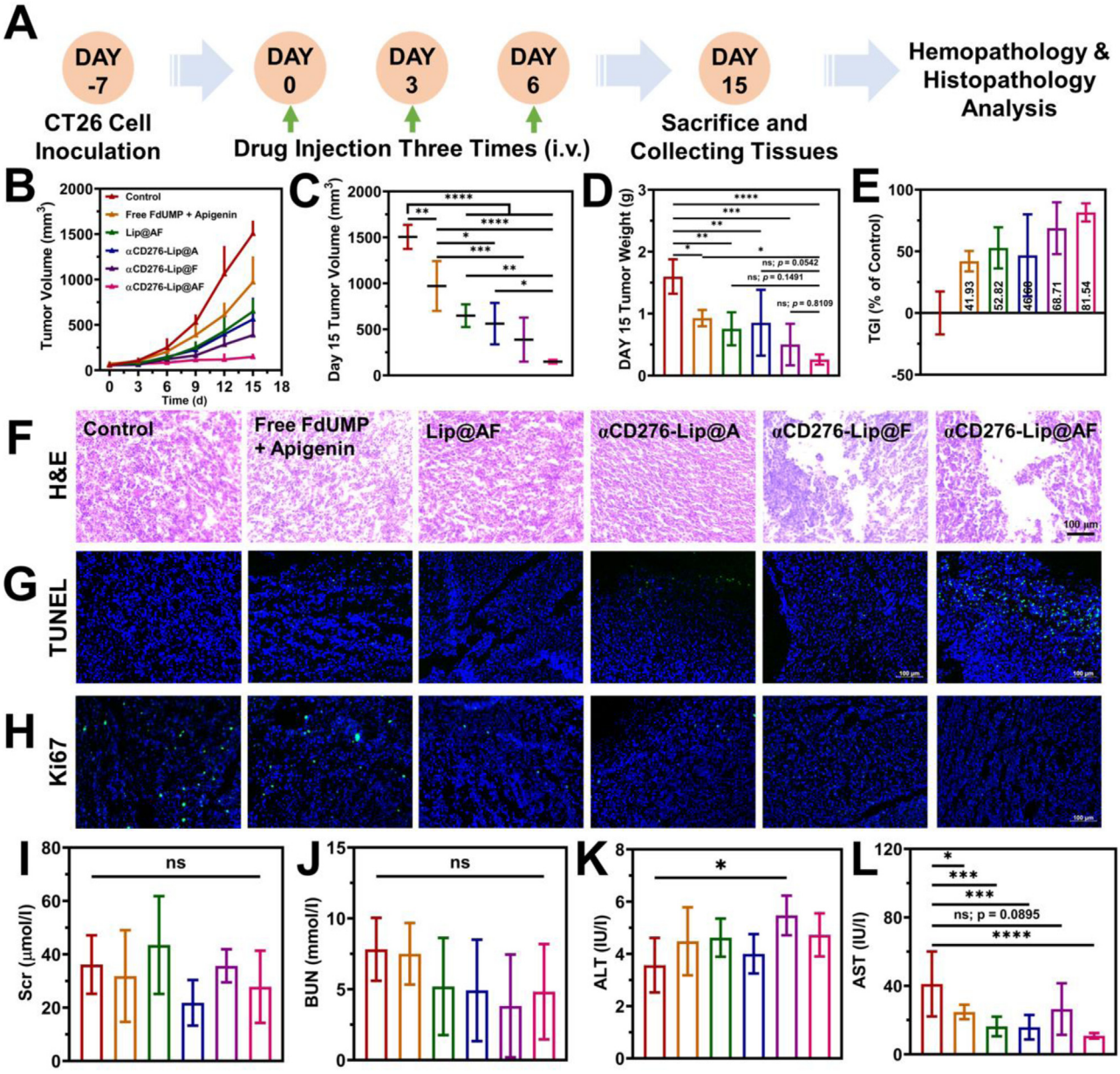

Fig. 5 – *In vivo* therapeutic evaluation of αCD276-Lip@AF. (A) Schematic illustration of *in vivo* evaluation procedure; (B) Tumor volume proliferation curves of tumors after different treatments ($n = 5$); (C) Tumor volumes in different groups at Day 15; (D) Tumor weights in different groups at Day 15; (E) TGI% in different groups; (F) H&E staining of tumor frozen sections (Scale bar: 100 μm); (G) TUNEL staining of tumor frozen sections (Scale bar: 100 μm); (H) Ki67 staining of tumor frozen sections (Scale bar: 100 μm); (I) Averaged Scr contents; (J) Averaged BUN contents; (K) Averaged ALT contents; (L) Averaged AST contents (ns: no significance, * $P < 0.05$, *** $P < 0.001$, **** $P < 0.0001$).

group, ~41.11 IU/l in control group, **** $P < 0.0001$) were all in the normal range, reflecting the minor toxicity and damage to liver and kidney. According to H&E staining results, no obvious damage was observed in heart, liver, spleen, lung and kidney tissues, verifying its safety to major organs.

4. Conclusion

Intracellular redox homeostasis plays a vital role in multiple bio-activities. Destroying redox balance could damage various organelles including cell membrane and mitochondria, leading to cellular activity disorder via different cell death mechanisms, eventually achieving efficient tumor cell killing. Inducing redox imbalance provides a promising strategy for anti-tumor treatment. Here in, apigenin and FdUMP were combined, redox balance was disrupted by depleting anti-oxidant GSH and inducing ROS, cell proliferation arrest and apoptosis could be achieved through DNA damage and energy shortage by GSH downregulation. Highly unbalanced redox environment leads to the decrease of mitochondria membrane potential, cell membrane lipid peroxidation

and cytoplasm outflow, DAMPs may be released and as a result immunogenicity of tumors was enhanced. Therefore, blockade of immune-checkpoint CD276 by antibody further promoted the recognition of immune cells to tumors. Lipid nanoparticles was designed for codelivery of apigenin, FdUMP, and αCD276 with rational particle size, achieving satisfied *in vivo* tumor accumulation. On the basis of the verified tumor killing and targeting ability, αCD276-Lip@AF exhibited efficient tumor growth inhibition with high biosafety. In conclusion, this work validated the combinational antitumor efficiency by destroying redox balance and blocking immune-checkpoint, provides new insights into the therapy of malignant tumors including CRC.

Conflicts of interest

The authors declare that they have no known competing financial interests or personal relationships that could have appeared to influence the work reported in this paper.

Acknowledgments

This work was financially supported by the National Natural Science Foundation of China (82173769), Tianjin Science Foundation for Distinguished Young Scholars (24JCJQJC00050), Applied Basic Research Multi-Investment Foundation of Tianjin (21JCYBJC01540), the National Natural Science Foundation of China (82300336), and the Science & Technology Development Fund of Tianjin Education Commission for Higher Education (2019KJ178).

Supplementary materials

Supplementary material associated with this article can be found, in the online version, at doi:10.1016/j.ajps.2025.101016.

References

[1] Ma P, Luo Z, Li Z, Lin Y, Li Z, Wu Z, et al. Mitochondrial artificial K^+ channel construction using MPTPP@5F8 nanoparticles for overcoming cancer drug resistance via disrupting cellular ion homeostasis. Adv Healthc Mater 2024;13(2):e2302012.
[2] Wang M, Ma PA, Lin J. Nanoplatform-based cellular reactive oxygen species regulation for enhanced oncotherapy and tumor resistance alleviation. Chinese Chem Lett 2023;34(9):108300.
[3] Ning P, Wang W, Chen M, Feng Y, Meng X. Recent advances in mitochondria- and lysosomes-targeted small-molecule two-photon fluorescent probes. Chinese Chem Lett 2017;28(10):1943–51.
[4] Jiang X, Stockwell BR, Conrad M. Ferroptosis: mechanisms, biology and role in disease. Nat Rev Mol Cell Biol 2021;22(4):266–82.
[5] Jin X, Tang J, Qiu X, Nie X, Ou S, Wu G, et al. Ferroptosis: emerging mechanisms, biological function, and therapeutic potential in cancer and inflammation. Cell Death Discov 2024;10(1):45.
[6] Catanzaro E, Demuynck R, Naessens F, Galluzzi L, Krysko DV. Immunogenicity of ferroptosis in cancer: a matter of context? Trends Cancer 2024;10(5):407–16.
[7] Vodenkova S, Buchler T, Cervena K, Veskrnova V, Vodicka P, Vymetalkova V. 5-Fluorouracil and other fluoropyrimidines in colorectal cancer: past, present and future. Pharmacol Ther 2020;206:107447.
[8] Bijnsdorp IV, Comijn EM, Padron JM, Gmeiner WH, Peters GJ. Mechanisms of action of FdUMP[10]: metabolite activation and thymidylate synthase inhibition. Oncol Rep 2007;18(1):287–91.
[9] Xie Y, Kang R, Klionsky DJ, Tang D. GPX4 in cell death, autophagy, and disease. Autophagy 2023;19(10):2621–38.
[10] Laberge RM, Karwatsky J, Lincoln MC, Leimanis ML, Georges E. Modulation of GSH levels in ABCC1 expressing tumor cells triggers apoptosis through oxidative stress. Biochem Pharmacol 2007;73(11):1727–37.
[11] Choi EJ, Kim GH. 5-Fluorouracil combined with apigenin enhances anticancer activity through induction of apoptosis in human breast cancer MDA-MB-453 cells. Oncol Rep 2009;22(6):1533–7.
[12] Chan LP, Chou TH, Ding HY, Chen PR, Chiang FY, Kuo PL, et al. Apigenin induces apoptosis via tumor necrosis factor receptor- and Bcl-2-mediated pathway and enhances susceptibility of head and neck squamous cell carcinoma to 5-fluorouracil and cisplatin. Biochim Biophys Acta 2012;1820(7):1081–91.
[13] Hu XY, Liang JY, Guo XJ, Liu L, Guo YB. 5-Fluorouracil combined with apigenin enhances anticancer activity through mitochondrial membrane potential ($\Delta\Psi$m)-mediated apoptosis in hepatocellular carcinoma. Clin Exp Pharmacol P 2015;42(2):146–53.
[14] Yang C, Song J, Hwang S, Choi J, Song G, Lim W. Apigenin enhances apoptosis induction by 5-fluorouracil through regulation of thymidylate synthase in colorectal cancer cells. Redox Biol 2021;47:102144.
[15] Johnston PG, Lenz HJ, Leichman CG, Danenberg KD, Allegra CJ, Danenberg PV, et al. Thymidylate synthase gene and protein expression correlate and are associated with response to 5-fluorouracil in human colorectal and gastric tumors. Cancer Res 1995;55(7):1407–12.
[16] Chu E, Koeller DM, Johnston PG, Zinn S, Allegra CJ. Regulation of thymidylate synthase in human colon cancer cells treated with 5-fluorouracil and interferon-gamma. Mol Pharmacol 1993;43(4):527–33.
[17] Swain SM, Lippman ME, Egan EF, Drake JC, Steinberg SM, Allegra CJ. Fluorouracil and high-dose leucovorin in previously treated patients with metastatic breast cancer. J Clin Oncol 1989;7(7):890–9.
[18] Peters GJ, Backus HHJ, Freemantle S, Van Triest B, Codacci-Pisanelli G, Van Der Wilt CL, et al. Induction of thymidylate synthase as a 5-fluorouracil resistance mechanism. Bba-Mol Basis Dis 2002;1587(2–3):194–205.
[19] Zekri L, Lutz M, Prakash N, Manz T, Klimovich B, Mueller S, et al. An optimized IgG-based B7-H3xCD3 bispecific antibody for treatment of gastrointestinal cancers. Mol Ther 2023;31(4):1033–45.
[20] Hu C, Wang S, Wang J, Ruan X, Wu L, Zhang Z, et al. B7-H3 enhances colorectal cancer progression by regulating HB-EGF via HIF-1α. J Gastrointest Oncol 2024;15(3):1035–49.
[21] Zhang T, Wang F, Wu JY, Qiu ZC, Wang Y, Liu F, et al. Clinical correlation of B7-H3 and B3GALT4 with the prognosis of colorectal cancer. World J Gastroenterol 2018;24(31):3538–46.
[22] Varghese E, Samuel SM, Brockmueller A, Shakibaei M, Kubatka P, Büsselberg D. B7-H3 at the crossroads between tumor plasticity and colorectal cancer progression: a potential target for therapeutic intervention. Cancer Metastasis Rev 2024;43(1):115–33.

[23] Hao YY, Li H, Ge XY, Liu Y, Yin JL, Li X, et al. Site-specific nanoswitch circumventing immune resistance via activating TLR and inhibiting PD-L1/PD-1 axis. J Control Release 2023;361:64–76.
[24] Hu X, Xu M, Hu Y, Li N, Zhou L. B7-H3, negatively regulated by miR-128, promotes colorectal cancer cell proliferation and migration. Cell Biochem Biophys 2021;79(2):397–405.
[25] Jin H, Zhu M, Zhang D, Liu X, Guo Y, Xia L, et al. B7H3 increases ferroptosis resistance by inhibiting cholesterol metabolism in colorectal cancer. Cancer Sci 2023;114(11):4225–36.
[26] Guo J, Yu Z, Sun D, Zou Y, Liu Y, Huang L. Two nanoformulations induce reactive oxygen species and immunogenetic cell death for synergistic chemo-immunotherapy eradicating colorectal cancer and hepatocellular carcinoma. Mol Cancer 2021;20(1):10.
[27] Oliveira JP, Prado AR, Keijok WJ, Antunes PWP, Yapuchura ER, Guimarães MCC. Impact of conjugation strategies for targeting of antibodies in gold nanoparticles for ultrasensitive detection of 17β-estradiol. Sci Rep 2019;9(1):13859.
[28] Yang H, Le QV, Shim G, Oh YK, Shin YK. Molecular engineering of antibodies for site-specific conjugation to lipid polydopamine hybrid nanoparticles. Acta Pharm Sin B 2020;10(11):2212–26.
[29] Lwin TM, Hernot S, Hollandsworth H, Amirfakhri S, Filemoni F, Debie P, et al. Tumor-specific near-infrared nanobody probe rapidly labels tumors in an orthotopic mouse model of pancreatic cancer. Surgery 2020;168(1):85–91.
[30] Su Z, Xiao D, Xie F, Liu L, Wang Y, Fan S, et al. Antibody–drug conjugates: recent advances in linker chemistry. Acta Pharmacol Sin B 2021;11(12):3889–907.
[31] Cao W, Zhang X, Li R, Li Z, Lu A, Yu F, et al. Lipid core-shell nanoparticles co-deliver FOLFOX regimen and siPD-L1 for synergistic targeted cancer treatment. J Control Release 2024;368:52–65.
[32] Cao W, Zhang X, Feng Y, Li R, Lu A, Li Z, et al. Lipid nanoparticular codelivery system for enhanced antitumor effects by ferroptosis-apoptosis synergistic with programmed cell death-ligand 1 downregulation. ACS nano 2024;18(26):17267–81.